



Design of CsI(Tl) detector system to search for lost radioactive source

Waseem Khan¹ · Chao-Hui He¹ · Qing-Min Zhang¹ · Yu Cao¹ · Wei-Tao Yang¹

Received: 14 February 2019 / Revised: 11 May 2019 / Accepted: 14 May 2019 / Published online: 12 August 2019
© China Science Publishing & Media Ltd. (Science Press), Shanghai Institute of Applied Physics, the Chinese Academy of Sciences, Chinese Nuclear Society and Springer Nature Singapore Pte Ltd. 2019

Abstract This report presents a design system based on the use of CsI(Tl) detectors to search for lost radioactive sources that are dangerous and harmful to individuals, including searching persons. For this purpose, the GEANT4 simulation toolkit was utilized to develop a system based on three detectors. Various simulated analyses were performed on the dose rates of the three detectors using different source–detector distances and detector separation. There were good agreement between the simulated results and the experimentally measured data. A new method was discussed to detect and search for radioactive sources based only on the dose rates in detectors with source activity. Numerical analyses were performed based on the measured dose rates and the difference of distances to determine the actual location of the lost single or multiple γ -ray sources at a specific angle. The detection limit was calculated from the background radiation to establish the sensitivity and capability of the proposed detector system. This system can be applied in fields in which it is necessary to locate unknown radioactive sources.

Keywords GEANT4 · γ -Ray source · CsI(Tl) detectors

This research was conducted at Xi'an Jiaotong University and was fully supported by key research and development plan of Shandong Province (No. 2017CXGC0916) and the Chinese government.

✉ Chao-Hui He
hechaohui@xjtu.edu.cn

¹ Department of Nuclear Science and Technology, School of Energy and Power Engineering, Xi'an Jiaotong University, Xi'an 710049, China

1 Introduction

Nuclear accidents that occur in power plants release numerous radioactive products into the environment. Cesium-137 is a major contributor to the total radiation released during nuclear accidents. The largest amounts of radio-cesium were released with an activity of 0.41×10^6 Ci and 2.3×10^6 Ci during the Fukushima and Chernobyl nuclear reactor explosion, respectively [1]. In many cases, if a radiation source is lost, it will produce deterministic and stochastic effects in the human body. To reduce the damage, searching for the lost radiation source is necessary. γ -ray spectrometry with a sensitive detector is widely used to monitor radioactive sources in radiation environments. In recent years, several techniques have been developed to identify and locate radioactive sources using γ -ray spectrometry. Hjerpe et al. [2] used a statistical method to locate a lost point source in the environment. In this method, different geometries were studied for the NaI(Tl) detector and the radioactive source was investigated. Aage and Korsbech [3] presented a Rainbow method to detect and identify lost radioactive sources based on noise-adjusted singular value decomposition and on area-specific stripping of the spectra. A semi-empirical method was proposed by Byun et al. [4] to detect radioactive sources. They used a portable HPGe gamma spectrometry system based on a virtual point detector concept. Results were presented for a ($34 \mu\text{Ci}$) ^{137}Cs source placed at 10 different positions from the detector system. Gamage et al. [5] discussed a scanning-based method to localize radioactive sources in a three-dimensional domain. An organic liquid scintillator detector was used to obtain the location of sources using a γ -ray imaging system. Several authors have used different approaches based on a single

radiation detector for source estimation, localization, and tracking, as well as the separation of multiple sources [6–9]. However, an additional detector was required to search for the location of the source [10]. Willis et al. [11] used a set of four radiation detectors in a four-quadrant formation to detect and identify γ -ray sources. A numerical approach was proposed with an external shield effect to determine the location of lost γ -ray source within 10.35° . A detector system was developed based on GEANT simulation by Akkoyun [10] for identification of γ -ray direction. The design comprised three quadratic NaI(Tl) scintillators that were perpendicular to each other. Based on the counts for each of the three detectors, the direction of γ -rays was obtained with a deviation angle of 2° . These techniques can be used to detect and locate a γ -ray source within a certain angle but cannot be used to quickly search for the location of radioactive sources within a small deviation angle. To improve the radiation detection and searching capability, a specialized spatial detector system should be developed.

In this work, a new detector system was designed to locate lost single or multiple radioactive sources. Based on the dose rate of three CsI(Tl) detectors, radiation sources were searched using a small deviation angle. We present various simulated analyses and the results of an experiment to verify the operation principles.

2 Materials and methods

CsI(Tl) is one of the brightest scintillators due to its high light output, which increases the signal and reduces the statistical uncertainty in position and energy. The appropriate matching between the CsI(Tl) and the photodiodes improve the energy resolution, which is useful for the identification of radioactive sources. Due to the high γ -ray stopping power, good radiation hardness properties and detection of ionizing radiation, CsI(Tl) has been extensively used for security applications, high energy physics, space research, and nuclear medicine. The main specifications of CsI(Tl) scintillators are summarized in Table 1.

2.1 Detector design

The detector was constructed with a (30 mm \times 10 mm \times 10 mm) cuboid cesium iodide (CsI) thallium (Tl) crystal and PIN photodiode (PD). The detector model was Ga-01, and its energy resolution at 662 keV ^{137}Cs was 6.1%. The performance specifications of the detector are given in Table 2. The detector was packaged in a steel shielded box with a thickness (0.3 mm), volume (45 mm \times 18 mm \times 24 mm), and high gain preamplifier to avoid the effect of β -rays. A schematic of the detector system is shown in Fig. 1.

Table 1 Some specifications of CsI(Tl) scintillators

	CsI(Tl)
Density (g/cm^3)	4.51
Peak emission (nm)	550
Decay constant (10^{-6} s)	1.30
Radiation length (cm)	1.9
Decay time (ns)	1000
Atomic number	54
Refractive index	1.79
Light yield (photons/ $\text{keV}\gamma$)	54
Hygroscopic	Slightly

Table 2 Performance specifications of the detector

Energy detection range	50 KeV
Power supply	2.7–3.3 V
Signal amplitude	$0.9 \text{ V} \pm 0.1 \text{ V}$
Detection efficiency	$25,000 \pm 20\%$ counts/ μSv
Working temperature	-20 to 50°C
Working life	5 years

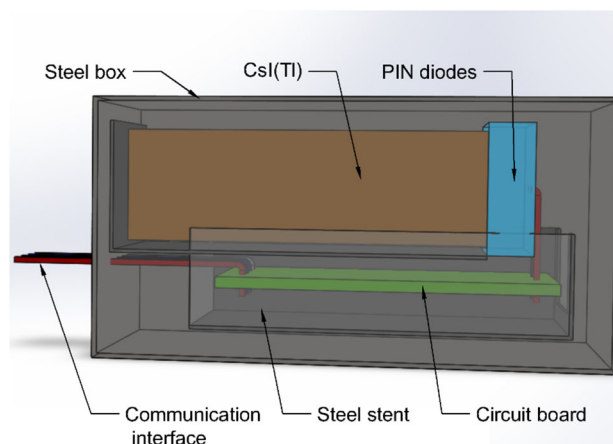


Fig. 1 CsI(Tl) detector with steel box (color online)

2.2 Basic principle

A single detector cannot easily locate the exact position of a γ -ray source. It is essential to design a system consisting of multiple detectors to quickly determine the location of a source. In this regard, a three-detector system was designed. In this system, each detector (CsI(Tl) PD with steel box) was labeled as A, B and C as shown in Fig. 2. The dose rate in detector B is used to determine the distance between the source and the system (D_{sd}) along the $-Z$ axis. The line between the source and detector B is

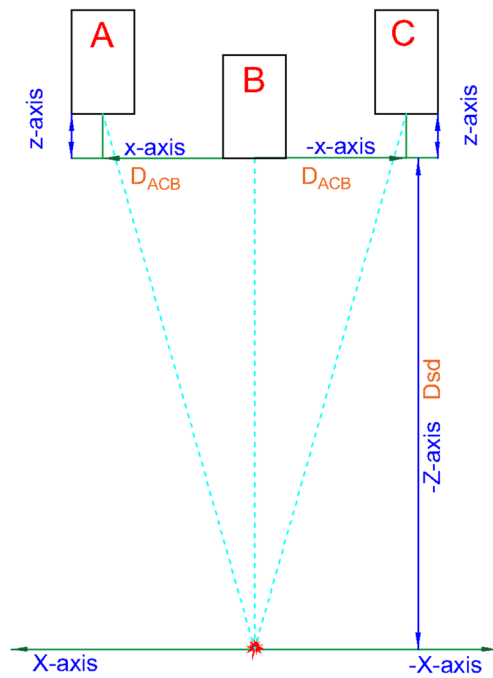


Fig. 2 Schematic of the source–detector. D_{sd} shows the distance between the source and the three detectors along the $-Z$ axis, and D_{ACB} is the distance between the detectors along the $\pm x$ axis and the z axis. The $\pm X$ axis is used to determine the deviation away from the axial position

called the axis. Detectors A and C are positioned on either side of detector B. They are used to determine the deviation away from the axis. The distance between detector B and detector A or C is called D_{ACB} , along the $\pm x$ axis and z axis. The deviation depends on the difference between the dose rates of detectors A and C. In a rare case, if the dose rates in detector A and C are equal, then there is no deviation from the axis and the dose rate in detector B only can be used to identify the position of the source. However, the difference of dose rates in detector A and C indicates that the radiation source is not on the axis. In this case, the deviation angle produced depends on the difference of the dose rates of detectors A and C. The bigger the difference, the larger the deviation angle. The absence of shields in the detectors can affect the identification of the source. Therefore, shields were placed around the detectors to minimize the effect of incoming and scattered γ -rays. The entire detector system was fixed in a metal case so that the radiation entered through only the front face of the detectors.

2.3 Electrical design

Each detector is connected with a cable of approximately 55 mm as the connection interface. The connector is a 4-pin MOLEX PicoBlade™ 1.25-mm (0.049")

connector (refers to Molex connector, part number 51021-0400). The pulse signal from the sensor is filtered using a pulse discriminator and then counted using a single-chip microcomputer (MSP430F169) linked with each connector. The single-chip microcomputer calculates the radiation intensity of the sensor surface according to the counting rate and issues an alarm when the radiation intensity exceeds the alarm value set by the microcomputer. The single-chip microcomputer is further connected via a USB port to transmit data to a laptop. The detectors and the connection scheme are shown in Fig. 3.

2.4 Experimental setup

The three-detector system with the appropriate circuitry was fixed in a steel metal case with a thickness (60 mm), a radius ($R = 20$ cm) and weight (12.18 kg) as shown in Fig. 4. The distance between the three detectors was set at (± 6 cm) along the $\pm x$ axis and (1.6 cm) along the z axis. Steel shields with a height of 18 mm and a width of 36 mm were inserted inside the metal case around the detectors. The designed system was equipped with a movable disk of thickness (18 mm) with an angular scale in degrees. The position of the designed system can be adjusted based on the angular scale. A cart was used to move the system forward, backward to make turning easier. Lead bricks of length 19 cm, diameter 10 cm, and thickness 3 cm were used around the radioactive source, except for one side. In the first set of experiments, a mono-energetic γ -ray source with an energy of 662 keV and activity of 0.37 GBq was used. The source was fixed at a specific position, and the dose rate was measured at various locations of the designed system. The measurements were taken for multiple γ -ray sources in two modes. In the first mode, two unknown radioactive sources were set 300 cm apart at two different positions (0° and 180°) around the system as shown in

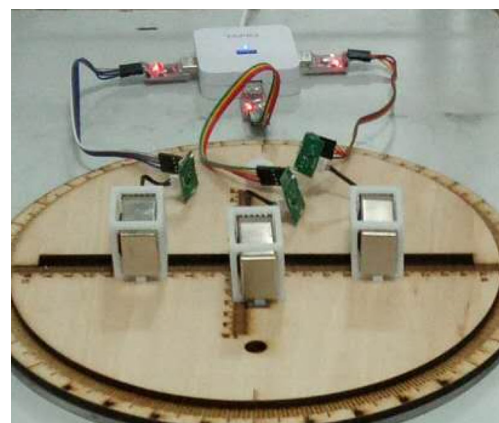


Fig. 3 CsI detectors and connection scheme of the system (color online)

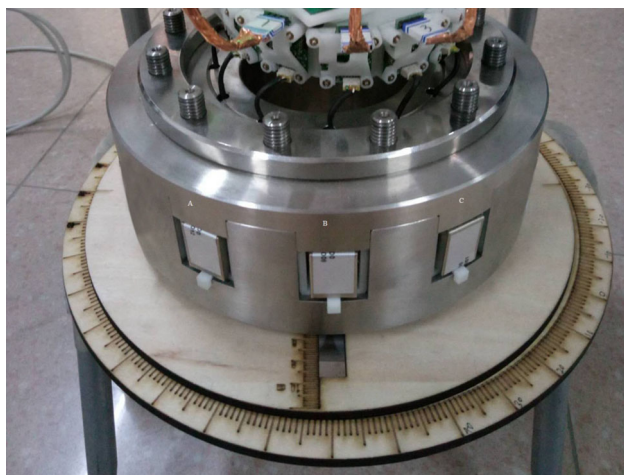


Fig. 4 Designed system for three detectors (color online)

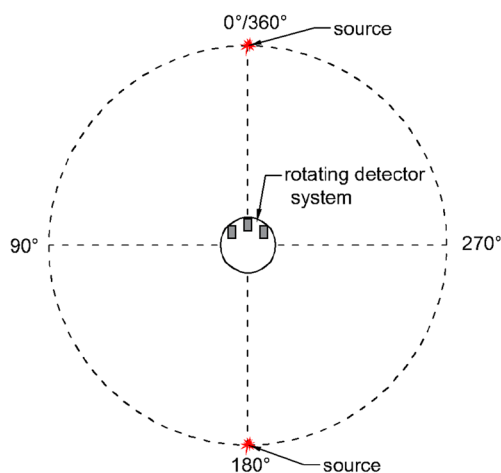


Fig. 5 Experimental setup for finding the direction of multiple γ -ray sources

Fig. 5. Measurements were obtained from 0° to 360° with an interval of 30° . After a complete rotation of the detector system, the recorded dose rates were plotted according to the observed detector angle and the various peaks that indicate the direction of the source. The locations of the lost multiple γ -ray sources were searched in the second mode. For this purpose, two unknown sources were simultaneously fixed at 0° and 90° at unknown distances from the designed system. Firstly, the dose rates were measured at two different positions. A measurement was acquired at 0° , then the system was rotated to 90° , and the dose rate was obtained. Based on the dose rates and the difference of the distance, the location of each lost source was determined. Equal dose rates were obtained for detectors A and C for the deviation angle for the first position of the designed system.

2.5 GEANT4 model

GEANT4 (GEometry ANd Tracking) [12], a general-purpose object-oriented toolkit for the simulation of particle detectors was used. In the simulation, the detailed physics treatment for photon interactions, such as the photoelectric effect, Compton effect, and pair production, was utilized. The generation of secondary electrons from photons was also considered. The largest number of primary photons was considered in each run to improve the statistical uncertainty associated with the simulated dose. An initial number of photons (10^7) was used for the simulation to maintain a relative statistical error of less than 0.5%. The default cutoff value defines the production threshold of secondary particles, corresponding to the stopping range of the particles; in our simulation, the production cutoff was set to 1 mm for both γ -rays and electrons. The simulated dose was defined as the energy deposited by all particles in a sensitive volume divided by the number of simulated γ -rays and the mass of the sensitive volume using the following equation:

$$\text{Dose } (\mu\text{Gy}) = \frac{E}{NM}, \quad (1)$$

where E is the energy deposited by all particles in a sensitive volume, N is the number of γ -ray photons, and M is the mass of the sensitive volume.

To obtain the value in $\mu\text{Gy/h}$, each simulated dose value was multiplied by 133,200/h with initial primary protons of (10^7) and activity of 0.37 GBq.

Three cuboid CsI(Tl) detectors with a steel cylinder were modeled, and the simulation was performed in two steps for the ^{137}Cs point source. Firstly, the source was fixed, and the simulated dose rates were obtained at various locations of the detector system along the $-Z$ axis. In the second case, the dose rate was simulated for different positions of two detectors along the $\pm x$ axis and z axis.

2.6 Experimental measurement

The measured data were analyzed using a Serial Port Utility software. The counting time for each detector and case was 3 min (can be adjusted), and a total of 36 counts were collected in c/s or $\mu\text{R/h}$ during this time. The total counts were averaged and multiplied by 9.999×10^{-3} to obtain the dose rate in $\mu\text{Gy/h}$. The counting dead times were always less than 3%, and consequently, a correction was performed during counting. Initially, the system was used to measure the background dose rates for the three detectors. At the maximum separation of the detectors and source, the background dose rates were measured ($0.156 \mu\text{Gy/h}$) with a relative statistical error ($\pm 0.0021 \mu\text{Gy/h}$). The measurements were taken by

searching for a point source in an area with a low and stable background. As such, there was no need for background correction. The standard error (SE) of the measurement was calculated as follows:

$$SE = \frac{s}{\sqrt{N}}, \tag{2}$$

where s is the standard deviation and N is the total number of counts for each detector for each of the different cases.

The relative deviation (RD) between the simulated and the experimental dose rate values is given by:

$$RD = \frac{\text{Experimental Dose rate} - \text{Simulated Dose rate}}{\text{Experimental Dose rate}} \times 100\%. \tag{3}$$

3 Results and discussion

3.1 Dose rates of detectors with different Dsd

The first analysis was performed based on the variation of the dose rate with the source–detector distance (Dsd) to examine the sensitivity of the designed system. The source was fixed and the dose rates were observed for the three detectors at different distances (200 cm, 300 cm, 400 cm, 500 cm, and 600 cm) of the designed system. The distance between the detectors (D_{ACB}) was (± 6 cm and 1.6 cm) along the $\pm x$ axis and z axis, respectively. Figure 6 shows the dependence of the dose rate value on Dsd with the standard error (vertical bar). When Dsd increases, the dose rates of the three detectors decrease. The dose rate of

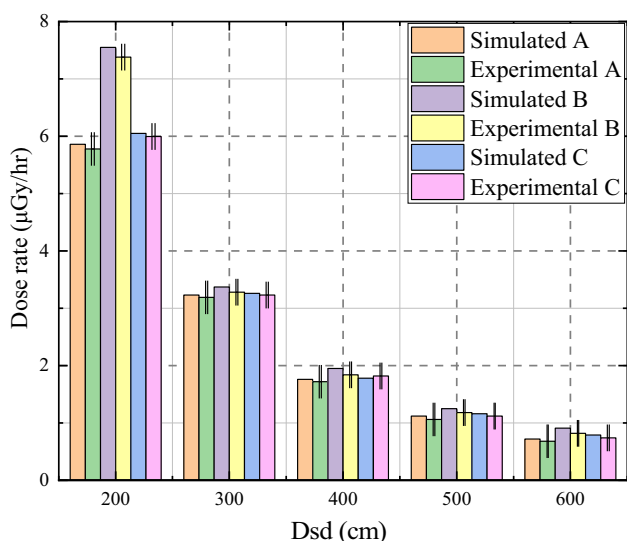


Fig. 6 Comparison of simulated and experimental dose rates for different Dsd (color online)

detector B at different Dsd was slightly greater than that of detectors A and C because it was closer to the source. The dose rates for detector A and C at each Dsd remained the same, but their dose rates decreased with the increase in Dsd. It is evident in Fig. 6 that the difference between the dose rates of detector A and C increases or decreases with the Dsd. Good agreement was obtained between the simulated and experimental results as shown in Fig. 7.

3.2 Dose rates in detectors on different D_{ACB}

To investigate the variation of the dose rates for the three detectors with D_{ACB} , an analysis was performed for different D_{ACB} (± 6 cm and ± 8 cm) along the $\pm x$ axis and (1.6 cm and 2 cm) along the z axis. The source was remained fixed at 300 cm along the $-Z$ axis. Figure 8 shows that the dose rates for detectors A and C slightly decrease with the increase in D_{ACB} . The shield was closer to detectors A and C at ± 6 cm and 1.6 cm along the $\pm x$ axis and z axis, respectively. Therefore, the maximum number of γ -ray photons was incident on detectors A and C. When D_{ACB} increased, the dose rates of detectors A and C decreased because at greater distances along the $\pm x$ axis and z axis to detector B, few γ -rays accumulated at detector A and Cs. Detector B remained fixed when detectors A and C were varied; therefore, the dose rate for detector B was observed to be the same. There was a good agreement between the simulated and experimental dose rates with a relative deviation (RD) 3% as shown in Fig. 9. The figure shows that the difference between the dose rates in detector A and C decreased at D_{ACB} (± 6 cm and 1.6 cm) along the $\pm x$ axis and z axis, respectively.

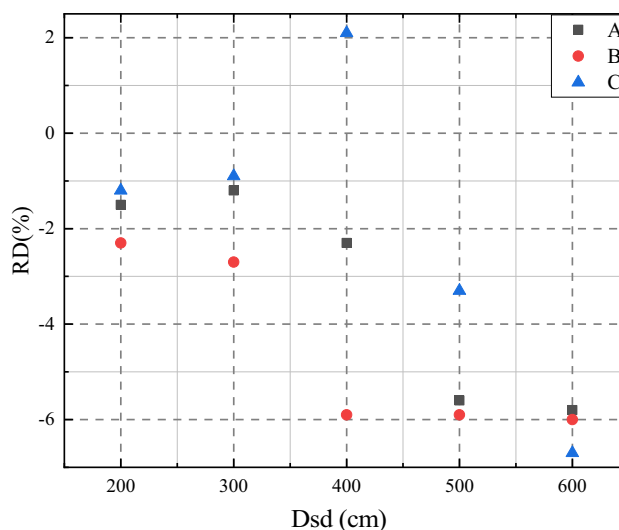


Fig. 7 Relative deviation of dose rates for different Dsd

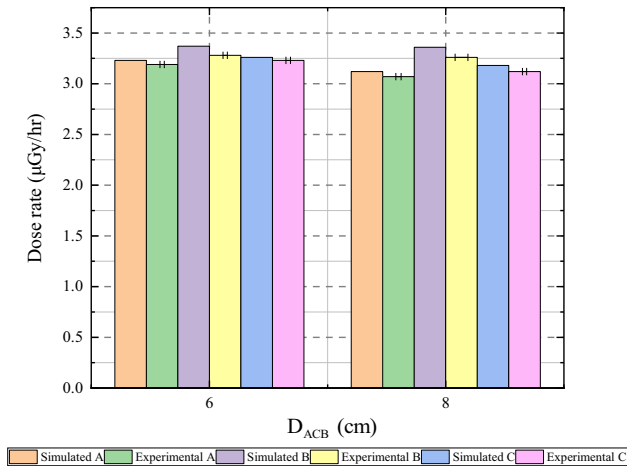


Fig. 8 Simulated and experimental dose rates for different D_{ACB} (color online)

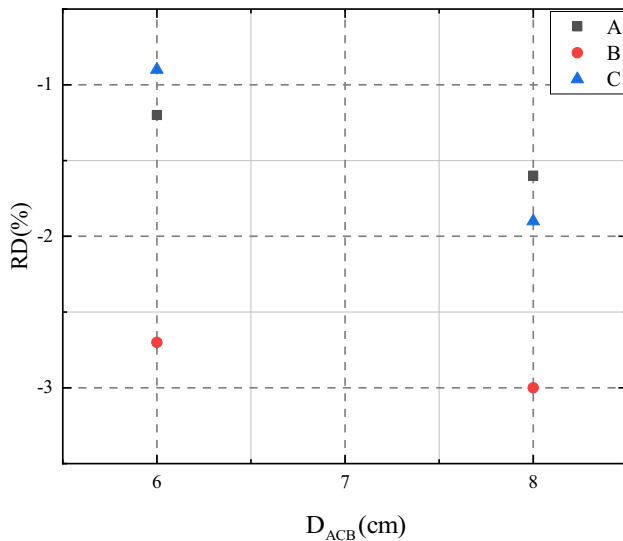


Fig. 9 Relative deviation of dose rates for different D_{ACB}

3.3 Dose rates in detectors on different angles (θ°)

The detectors were fixed at $D_{ACB}(\pm 6 \text{ cm and } 1.6 \text{ cm})$ along the $\pm x$ axis and z axis, respectively. The possible locations of the multiple γ -ray sources were searched based on the dose rates obtained by the detectors. Figure 10 shows that the maximum dose rates were observed at 0° , where the incident γ -rays are parallel to the three detectors. When the detector system rotates with the increasing angle, the dose rates for the three detectors become zero at 90° wherein the incident γ -rays are perpendicular to the three detectors. After a rotation of 180° , the dose rates of the detectors increased because of the second source. The same process was repeated, and a third peak was observed at 360° . The photopeaks in Fig. 10 show the directions of the two γ -ray sources. Figure 10 also shows that the difference

in the dose rates for detectors A and C increases with the deviation angle. This means that the deviation angle of the source can be determined from the difference of the dose rates for detectors A and C.

3.4 Analysis of the search for the γ -ray source

The sensitivity of the designed system was analyzed. In Fig. 6, the dose rates of the three detectors at Dsd (200 cm) were $(5.77 \pm 0.0126 \mu\text{Gy/h})$ for A, $(7.38 \pm 0.0139 \mu\text{Gy/h})$ for B and $(5.99 \pm 0.0134 \mu\text{Gy/h})$ for C. The dose rate for detector B was used to determine the source location as follows:

$$D = \frac{AEI \mu_{en}}{4\pi r^2 \rho}, \tag{4}$$

$$r^2 = \frac{AEI \mu_{en}}{4\pi D \rho}, \tag{5}$$

$$r = \sqrt{\frac{AEI \mu_{en}}{4\pi D \rho}}, \tag{6}$$

where D is the dose rate ($\mu\text{Gy/h}$), E is the energy per decay (662 keV), I is the γ -ray emission probability (89.9%), A is the radioactivity (0.37 GBq) at the time of the measurement, and $\frac{\mu_{en}}{\rho}$ is the mass energy-absorption coefficient of air ($29.5 \text{ cm}^2/\text{kg}$).

The difference between the dose rates of detectors A and C shows that the source was not on the axis. The dose rate in detector A was less than that of detector C, so the designed system was slightly displaced with an angle toward detector C to obtain the equal dose rates for both detectors. The angle was the deviation of the source away from the axis. The deviation angle was approximately 1.71° and dependent on the difference between the dose rates in detectors A and C. The angle of deviation was obtained as follows:

$$\theta = \tan^{-1} \frac{X}{Z} \tag{7}$$

The dose rate for detectors B was greater than that of detector C, so the source was closer to detector B. The source was between ($r(-) = 200.22 \text{ cm}$ and $r(+) = 199.90 \text{ cm}$) along the $-Z$ axis at $-X = 6 \text{ cm}$.

The location of the γ -ray source was searched at different positions (300 cm, 400 cm, 500 cm, and 600 cm) from the source using the designed system. The system was moved to different distances (1 cm, 1 cm, 1.5 cm, and 2.4 cm) along the $-X$ axis to obtain the equal dose rates for detectors A and C. The corresponding deviation angles and locations of the source are shown in Fig. 11. The Dsd results are in agreement with the actual positions, and the deviation angle is small.

Fig. 10 Experimental dose rates for the three detectors at different angles showing the directional sensitivity of multiple γ -ray sources (color online)

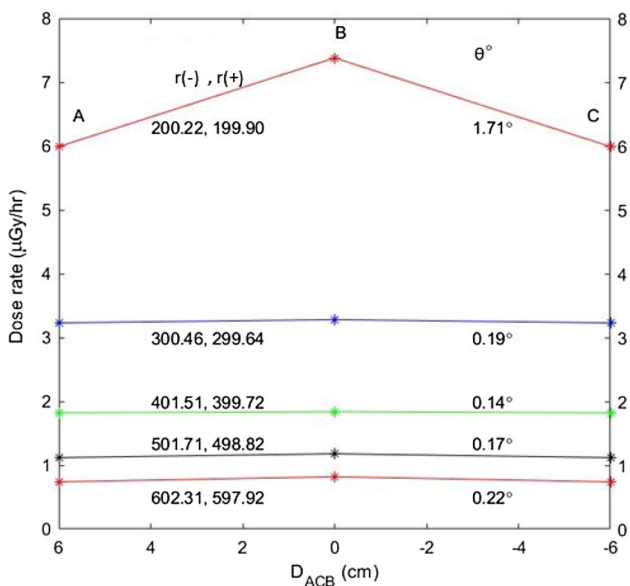
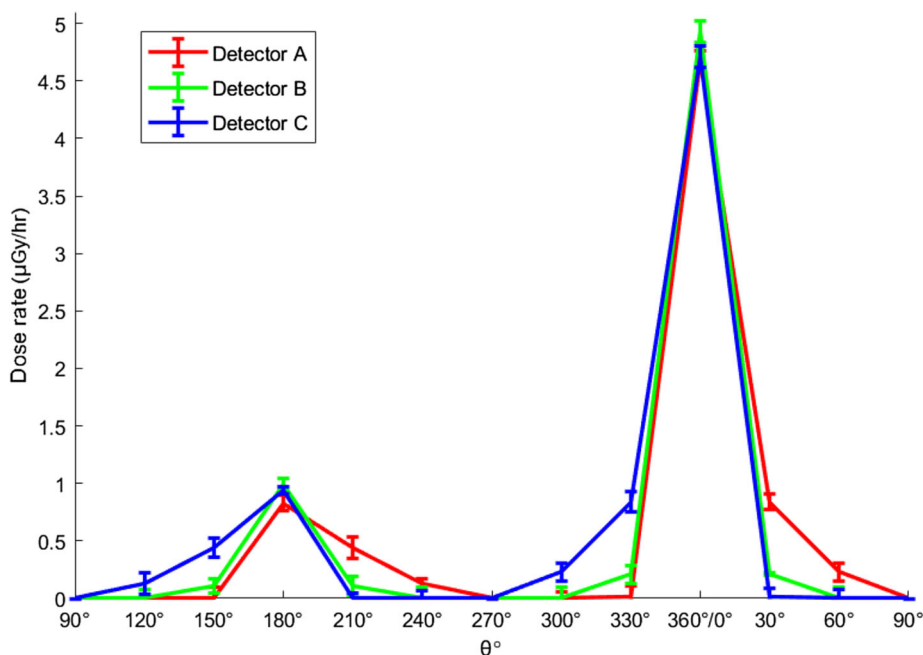


Fig. 11 Results of the actual location of the γ -ray source (color online)

Numerical analyses were performed based on the experimental results for searching for the γ -ray source without source activity. The location of the source was discussed based on the dose rates of the three detectors at two different distances. Initially, the dose rates in three detectors were observed at 300 cm and 200 cm. The dose rate at 300 cm is defined as follows:

$$D_1 = \frac{AEI}{4\pi r_1^2} \frac{\mu_{en}}{\rho} \tag{8}$$

The dose rate at 200 cm is given as follows:

$$D_2 = \frac{AEI}{4\pi(r_1 - \Delta)^2} \frac{\mu_{en}}{\rho} \tag{9}$$

Solving Eqs. 8 and 9, we obtain the following:

$$\left(\frac{D_1}{D_2} - 1\right) r_1^2 + 2\Delta r_1 - \Delta^2 = 0 \tag{10}$$

using the quadratic equation given as:

$$r_1 = \frac{-\Delta + \Delta \sqrt{\frac{D_1}{D_2}}}{\frac{D_1}{D_2} - 1}, \tag{11}$$

$$r_1 = \frac{-\Delta - \Delta \sqrt{\frac{D_1}{D_2}}}{\frac{D_1}{D_2} - 1} \tag{12}$$

Both equations were used to determine the location of the lost source, where Δ is the difference between the distances.

D_1 : Dose rate for detector B at 300 cm ($3.28 \pm 0.009 \mu\text{Gy/h}$)

D_2 : Dose rate for detector B at 200 cm ($7.38 \pm 0.0139 \mu\text{Gy/h}$)

Therefore, the position of the source was (r_1 (+)) = 299.80 cm and r_1 (-) = 299.13 cm using Eq. 12. For the verification of these results, first the source activity

(A (+) = 0.371 GBq and A (-) = 0.369 GBq) was obtained as follows:

$$A(\pm) = \frac{4\pi r_1^2(\pm)\rho D_1}{EI\mu_{en}}. \quad (13)$$

At source activity $A (+) = 0.371$ GBq and distance $r_1 (+) = 299.80$ cm, the dose rate ($D_2 (+) = 7.39$ $\mu\text{Gy/h}$) was obtained using Eq. 9 and a good agreement was observed in comparison with the direct experimental dose rate obtained for detector B at 200 cm. The deviation angle ($\theta^\circ = 0.19^\circ$) was obtained from the equal dose rates for detector A and C at 300 cm. Similarly, the analysis was performed for 400 cm and 300 cm distances. In these cases, the position of the source was approximately $r_1 (+) = 398.51$ cm, $r_1 (-) = 396.39$ cm, the source activity ($A (+) = 0.368$ GBq and $A (-) = 0.364$ GBq), the dose rate $D_2 (+) = 3.28$ $\mu\text{Gy/h}$ and the deviation angle ($\theta = 0.14^\circ$). The deviation angles for 500 cm and 600 cm were ($\theta = 0.17^\circ$) and ($\theta = 0.22^\circ$), respectively. This method only depends on the dose rates and the difference between the distances. It is very useful, especially when searching for the location of the lost sources.

Using the same methodology the lost γ -ray source was searched at different locations. For this purpose, a designed system was placed in an empty room that detects and searches for the radioactive source, as shown in Fig. 12. Firstly, the dose rates (0.37 ± 0.022 $\mu\text{Gy/h}$) for A, (0.43 ± 0.035 $\mu\text{Gy/h}$) for B and (0.40 ± 0.030 $\mu\text{Gy/h}$) for

C, were obtained at 1 position of the designed system, then at 3 positions. The dose rates were (0.75 ± 0.039 $\mu\text{Gy/h}$) for A, (0.90 ± 0.054 $\mu\text{Gy/h}$) for B and (0.79 ± 0.053 $\mu\text{Gy/h}$) for C. The difference between the distances of the two positions was 150 cm. Based on the dose rates in detector B, the lost γ -ray source was searched at (495.94 cm (+) and 472.29 cm (-)) using Eq. 12. To verify the result, the designed system was placed at 2 position and the dose rates were determined as (0.71 ± 0.031 $\mu\text{Gy/h}$) for A, (0.76 ± 0.050 $\mu\text{Gy/h}$) for B and (0.64 ± 0.038 $\mu\text{Gy/h}$) for C. The location of the source for 1 and 2 positions was (511.83 cm (+) and 462.62 cm (-)) with a difference of 120 cm. For 2 and 3 positions, the source location was (384.28 cm (+) and 359.24 cm (-)) with a difference of 30 cm. The total distance of the source from the 2 position was (504.28 cm (+) and 479.24 cm (-)) at 120 cm. These results show a good agreement with the source location of 1 and 3 positions. The actual location of the lost γ -ray source was obtained for the 1 position of the designed system with a deviation angle of 0.11° .

For multiple lost γ -ray sources, the dose rates for the detectors at the two positions were A (0.25 ± 0.016 $\mu\text{Gy/h}$), B (0.30 ± 0.017 $\mu\text{Gy/h}$) and C (0.27 ± 0.015 $\mu\text{Gy/h}$) and A (0.41 ± 0.022 $\mu\text{Gy/h}$), B (0.51 ± 0.028 $\mu\text{Gy/h}$) and C (0.46 ± 0.0149 $\mu\text{Gy/h}$) for source 1 at 0° with a difference of 100 cm. For the 90° position of the source, the dose rates were A (0.72 ± 0.021 $\mu\text{Gy/h}$), B (0.88 ± 0.042 $\mu\text{Gy/h}$) and C (0.87 ± 0.023 $\mu\text{Gy/h}$) and A (1.40 ± 0.031 $\mu\text{Gy/h}$), B (1.70 ± 0.041 $\mu\text{Gy/h}$) and C (1.56 ± 0.045 $\mu\text{Gy/h}$). The locations of the lost γ -ray sources were (430.30 cm (+) and 427.75 cm (-)) and (367.58 cm (+) and 349.12 cm (-)) with deviation angles of 0.06° and 0.15° , respectively.

Apart from the angle of deviation limit, the detection limit (the longest distance from the source that the detectors can detect the radiation) of the system was determined based on the background radiation dose rate. The dose rates for the three detectors remained the same (0.156 ± 0.0021 $\mu\text{Gy/h}$) at the longest distance D_{sd} (1385.22 cm (-), 1366.69 cm (+)). The detection limit depends on the background dose rate and the characteristics of the detector and characterizes the sensitivity of the system.

4 Conclusion

A detector system was designed based on the GEANT4 simulation toolkit to search for γ -ray sources. Numerical analyses were conducted to determine the location of lost single and multiple γ -ray sources. The method is based on the measurement of the dose rates of the three detectors and

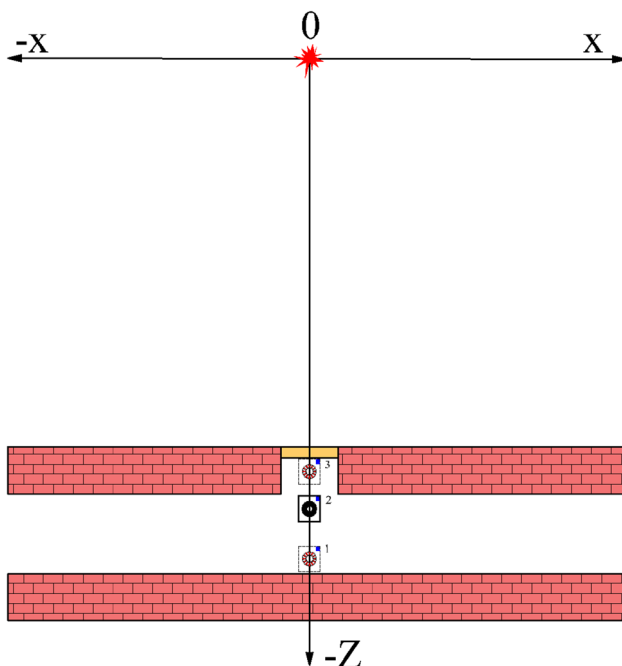


Fig. 12 Searching for the lost γ -ray source based on three positions of the designed system. The star represents a source, and the numbers 1, 2 and 3 represent the positions of the system

the difference between the distances. The outcomes indicate that the exact position of the γ -ray source was obtained with a small deviation angle. To achieve high sensitivity in the designed system, several analyses were performed based on the dose rate as a function of the source–detector distance and the distance between the detectors. The proposed system is useful in terms of searching for radioactive sources in a radiation environment and has a wide variety of applications such as in determining the leakage of radiation materials and in the identification of lost radioactive sources in metallic scrap prior to recycling.

Acknowledgements The authors would like to thank the entire staff of the Nuclear Science and Technology Department for providing valuable information in the completion of this work.

References

1. S.N.A. Sulaiman, F. Mohamed, A.N. Ab Rahim, Radioactive release during nuclear accidents in Chernobyl and Fukushima, in *IOP Conference Series: Materials Science and Engineering*. (IOP Publishing, 2018), 012011. <https://doi.org/10.1088/1757-899X/298/1/012011>
2. T. Hjerpe, R.R. Finck, C. Samuelsson, Statistical data evaluation in mobile gamma spectrometry: an optimization of on-line search strategies in the scenario of lost point sources. *Health Phys.* **80**, 563–570 (2001). <https://doi.org/10.1097/00004032-200106000-00006>
3. H.K. Aage, U. Korsbech, Search for lost or orphan radioactive sources based on NaI gamma spectrometry. *Appl. Radiat. Isot.* **58**, 103–113 (2003). [https://doi.org/10.1016/S0969-8043\(02\)00222-1](https://doi.org/10.1016/S0969-8043(02)00222-1)
4. J.-I. Byun, H.-Y. Choi, J.-Y. Yun, A 4-point in situ method to locate a discrete gamma-ray source in 3-D space. *Appl. Radiat. Isot.* **68**, 370–377 (2010). <https://doi.org/10.1016/j.apradiso.2009.10.054>
5. K. Gamage, M. Joyce, G. Taylor, Investigation of three-dimensional localisation of radioactive sources using a fast organic liquid scintillator detector. *Nucl. Instrum. Methods Phys. Res. A* **707**, 123–126 (2013). <https://doi.org/10.1016/j.nima.2012.12.119>
6. A.H. Zakaria, Y.M. Mustafah, J. Abdullah et al., Development of autonomous radiation mapping robot. *Procedia Comput. Sci.* **105**, 81–86 (2017). <https://doi.org/10.1016/j.procs.2017.01.203>
7. E. Wilhelm, S. Gutierrez, S. Ménard, Study of different filtering techniques applied to spectra from airborne gamma spectrometry. *J. Environ. Radioact.* **164**, 268–279 (2016). <https://doi.org/10.1016/j.jenvrad.2016.08.003>
8. J. Towler, B. Krawiec, K. Kochersberger, Radiation mapping in post-disaster environments using an autonomous helicopter. *Remote Sens.* **4**, 1995–2015 (2012). <https://doi.org/10.3390/rs4071995>
9. A. Miller, R. Machafi, A. Mohany, Development of a semi-autonomous directional and spectroscopic radiation detection mobile platform. *Radiat. Meas.* **72**, 53–59 (2015). <https://doi.org/10.1016/j.radmeas.2014.11.009>
10. S. Akkoyun, A method for determination of gamma-ray direction in space. *Acta Astronaut.* **87**, 147–152 (2013). <https://doi.org/10.1016/j.actaastro.2013.02.012>
11. M.J. Willis, S.E. Skutnik, H.L. Hall, Detection and positioning of radioactive sources using a four-detector response algorithm. *Nucl. Instrum. Methods Phys. Res. A* **767**, 445–452 (2014). <https://doi.org/10.1016/j.nima.2014.08.033>
12. S. Agostinelli, J. Allison, K. Amako et al., GEANT4: a simulation toolkit. *Nucl. Instrum. Methods Phys. Res. A* **506**, 250–303 (2003). [https://doi.org/10.1016/S0168-9002\(03\)01368-8](https://doi.org/10.1016/S0168-9002(03)01368-8)